THE ASTROPHYSICAL JOURNAL, 579:430–436, 2002 November 1

OCCULTATION AND MICROLENSING

ERIC AGOL[1,2]

Received 2002 June 19; accepted 2002 July 15

ABSTRACT

Occultation and microlensing are different limits of the same phenomenon of one body passing in front of another body. We derive a general exact analytic expression that describes both microlensing and occultation in the case of spherical bodies with a source of uniform brightness and a nonrelativistic foreground body. We also numerically compute the case of a source with quadratic limb darkening. In the limit that the gravitational deflection angle is comparable to the angular size of the foreground body, both microlensing and occultation occur as the objects align. Such events can be used to constrain the size ratio of the lens and source stars, the limb-darkening coefficients of the source star, and the surface gravity of the lens star (if the lens and source distances are known). Application of these results to microlensing during transits in binaries and giant-star microlensing is discussed. These results unify the microlensing and occultation limits and should be useful for rapid model fitting of microlensing, eclipse, and "micro-occultation" events.

Subject headings: binaries: eclipsing — eclipses — gravitational lensing — occultations

1. INTRODUCTION

When two stars (or other bodies) come into close alignment on the sky, the foreground star may either eclipse or microlens the background star. As the stars align, if the angular size of the foreground star is much larger than its gravitational deflection angle, then the foreground star can eclipse; if the contrary is true, then it can magnify. More precisely, gravitational lensing by a point mass produces two images of a distant object, one interior and one exterior to the Einstein radius in the lens plane, $R_E = [4R_g D_l(D_s - D_l)/D_s]^{1/2}$ where $R_g = GM/c^2$ is the gravitational radius for a lens of mass M, and $D_{l,s}$ are the distances to the lens or source. Both images move toward the Einstein radius as the lens and source approach, so the outer image will be occulted during the approach if the radius of the lens is larger than the Einstein radius. The inner image, however, starts off near the origin and thus is occulted when the source is far from the lens. As the lens and source approach, the inner image can become unocculted if the lens is smaller than the Einstein radius (Fig. 1). Occultation is most important in microlensing if $R_E \sim R_l$, where R_l is the radius of the lens star (assumed to be spherical). In Galactic microlensing, typically $R_l \ll R_E$, so occultation of the inner image occurs but is usually rather faint. In special circumstances, such as in eclipsing binaries containing compact objects (Maeder 1973; Marsh 2001) or lensing by giant stars, $R_l \sim R_E$, so the effects of both microlensing and occultation must be included. This "micro-occultation" can show more varied behavior than the usual microlensing or occultation light curves and can be used to constrain the surface gravity of the lens star (Bromley 1996).

Maeder (1973) and Marsh (2001) have carried out numerical computations of micro-occultation light curves. Here we present an exact *analytic* solution for the light curve of a uniform source that agrees with their work, and we present numerical calculations for limb-darkened sources. Bromley (1996) and Bozza et al. (2002) computed light curves for lensing events, treating the source as a point source, while the expressions presented here are valid for extended and limb-darkened sources as well. In § 2 we discuss microlensing and occultation of a point source. In § 3 we include the finite size of a uniform source. In § 4 we include the effects of limb darkening numerically for microlensing and occultation. In § 5 we apply the results to several astrophysical cases of possible interest, namely, white dwarf–main-sequence binaries, microlensing in globular clusters, and microlensing by supergiants. In § 6 we summarize.

2. POINT SOURCE

The lensing equation for a point source and point lens, neglecting diffraction and strong relativistic effects, is (Schneider, Ehlers, & Falco 1992)

$$\beta = \theta - \frac{1}{\theta} , \tag{1}$$

where θ and β are the image and source position angles in units of R_E/D_l. In the limit that the source is much smaller than the Einstein radius and is not aligned with the lens, then the point-source magnification is an adequate approximation (Paczyński 1986). Solving this equation, the image positions are

$$\theta_\pm = \tfrac{1}{2}(\beta \pm \sqrt{4+\beta^2}) , \tag{2}$$

where θ_- is the image interior to the Einstein radius and θ_+ is the image exterior to the Einstein radius ($|\theta_-| < 1$ and $\theta_+ > 1$). The magnifications of the images are

$$\mu^p_\pm = \frac{1}{2}\left(\frac{2+\beta^2}{\beta\sqrt{4+\beta^2}} \pm 1\right) , \tag{3}$$

or $\mu^p_+ = (1-\theta_+^{-4})^{-1}$ and $\mu^p_- = (1-\theta_-^4)^{-1}$.

If the size of the lens star is less than the size of the Einstein radius, $r_l = R_l/R_E < 1$, then the inner image will be occulted for $|\theta_-| < r_l$. This corresponds to $\beta > r_l^{-1} - r_l$, which means that the inner image is occulted when the source is distant from the lens and unoccults when the

[1] Chandra Fellow.

[2] California Institute of Technology, MS 130-33, Pasadena, CA 91125; agol@tapir.caltech.edu.

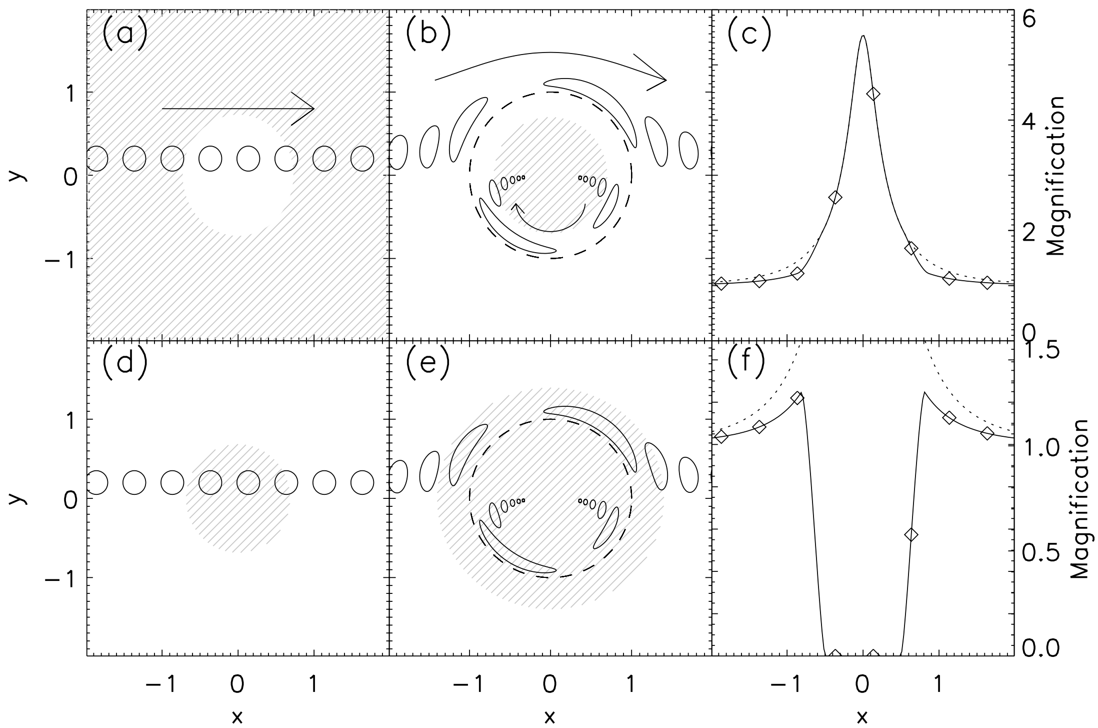

FIG. 1.—(*a*) Stars at various positions in the source plane. The shaded region shows the area in which the inner image is occulted by the lens star for $r_l < 1$, which is the region $\beta > \beta_l = 1/r_l - r_l$. The axes have units of $R_{\rm E} D_s/D_l$. (*b*) Images of the star in the image plane. The arrow is imaged as well for reference. The dashed line shows $R_{\rm E}$. (*c*) Magnification as a function of position. The dotted line shows the case with no occultation, while the solid line shows the case including occultation. The symbols show the magnification of the source at the positions depicted in (*a*). (*d*)–(*f*) Same as (*a*)–(*c*), but for $r_l > 1$. In this case, the inner image is fully occulted, and the shaded region in (*d*) shows where the outer image is occulted by the lens star.

source approaches the lens. The change in magnitude at the point of the occultation of the inner image is

$$\Delta m = -2.5 \log\left[1 + \frac{r_l^4}{1 + f(1 - r_l^4)}\right] , \qquad (4)$$

where $f = F_l/F_s$ is the ratio of the flux from the lens to the unlensed flux from the source. In typical Galactic microlensing events, $r_l \ll 1$, so the inner image usually appears (unoccults) when the source is distant from the lens, so the change in magnitude is very small. However, if the images can be resolved directly and the demagnified inner image is brighter than the lens star, then the appearance of the inner image might be detectable.

If the size of the lens star is greater than the Einstein radius, $r_l > 1$, then the inner image will always be occulted, and the outer image will be occulted for $\theta_+ < r_l$, which corresponds to $\beta < r_l - r_l^{-1}$. During occultation, the source star disappears so that one can only see the lens star. Thus, the total magnification for microlensing of a point source is

$$\mu^p = \mu_+^p \Theta\left(r_l \beta - r_l^2 + 1\right) + \mu_-^p \Theta\left(1 - r_l^2 - r_l \beta\right) , \qquad (5)$$

where

$$\Theta(x) = \begin{cases} 1, & x > 0 , \\ 0, & x \le 0 , \end{cases} \qquad (6)$$

is the step function. In the limit $r_l = 0$, this reduces to the usual microlensing magnification (Paczyński 1986), while in the limit $r_l \gg 1$, μ_-^p is negligible, $\mu_+^p \sim 1$, and occultation simply occurs when $\beta < r_l$.

At the point of occultation, $\beta = \pm\left(r_l^{-1} - r_l\right)$, and since β can be measured from a fit to the microlensing light curve, one can measure r_l (Bromley 1996). The sign is determined by whether the image appears (+) or disappears (−) at the center of the event.

The average astrometric position of the images during the microlensing event is (Walker 1995)

$$\Delta\theta = \frac{\mu_+^p \theta_+ + \mu_-^p \theta_-}{\mu^p + f} , \qquad (7)$$

where the difference in image position is measured with respect to the position of the lens on the sky. When $r_l < 1$, then the change in position during occultation of the inner image is

$$\Delta\theta(r_l) = -\frac{r_l^3}{(1+f)^2} . \qquad (8)$$

This has a weaker dependence on r_l than the magnitude change but is still quite small unless $r_l \sim 1$. In the case where $r_l > 1$, the source is completely occulted, so the centroid change is simply

$$\Delta\theta(r_l) = \frac{r_l}{f+1} . \qquad (9)$$

The point-source approximation has two limitations: during eclipse ingress or egress, the finite size of the source causes a smooth transition, and if the surface brightness of the source and lens are similar and $r_l \sim 1$, then the source must also have a size similar to the Einstein radius to contribute a significant fraction of the flux. Thus, in § 3 we derive a more general formula including the finite extent of the source.

3. EXTENDED UNIFORM SOURCE

In the case of a circular source with uniform surface brightness, the images may be partly or fully eclipsed by the lens star. The magnification (or dimming) is equal to the ratio of the unocculted area of the images to the area of the unlensed source, since surface brightness is conserved during lensing. For a uniform source, the area can be computed by integrating over the image boundaries using Stokes' theorem (Gould & Gaucherel 1997; Dominik 1998). In the case of a point-mass lens, this integral can be solved analytically, as first shown by Witt & Mao (1994) for $r_l = 0$. For an extended source with normalized radius

$$r_s = \frac{R_s D_l}{R_{\rm E} D_s} , \tag{10}$$

it is more useful to define a two-dimensional lensing equation to integrate over the source. Witt & Mao (1994) define a complex lensing equation

$$\zeta = z - \frac{1}{\bar{z}} , \tag{11}$$

where ζ is the complex coordinate for the source plane in units of $R_{\rm E} D_s / D_l$ and $z = x + iy$ is the complex coordinate for the lens plane in units of $R_{\rm E}$. Comparing with equation (1), $|\beta| = |\zeta|$ and $|\theta| = |z|$.

We assume that the source has a uniform surface brightness in the region $\zeta_0 + re^{i\phi}$ (ζ_0 is real and positive), where $0 \le \phi < 2\pi$ and $0 \le r \le r_s$, while we assume that the lens is opaque in the region $0 \le |z| \le r_l$. The solution for the image positions is

$$z_\pm = \frac{\zeta}{2}\left(1 \pm \sqrt{1 + \frac{4}{\zeta\bar{\zeta}}}\right) , \tag{12}$$

which is the complex version of equation (2). The lensing magnification for a uniform source is simply the ratio of the area of the lensed images to the area of the source. The integral over area can be converted to an integral over the source boundary using Stokes' theorem (Gould & Gaucherel 1997), giving

$$\mu_\pm = \pm \frac{1}{\pi r_s^2} \int d\phi |z_\pm|^2 \frac{\partial \Psi}{\partial \phi} , \tag{13}$$

where $\Psi = \cot^{-1}(\zeta_0 r_s^{-1} \csc\phi + \cot\phi)$ is the position angle of the image. The total magnification is

$$\mu = \mu_+ + \mu_- . \tag{14}$$

In the case of a finite-sized lens, $z_\pm$ should be replaced in the integrand with $r_l e^{i\Psi}$ whenever $|z_\pm| \le r_l$. In other words, when an image is partially occulted, then the inner boundary is given by the edge of the lens, while the outer boundary is given by the edge of the outer image.

There are several different cases to consider:

1. $r_s = 0$.—Point source (eq. [5]).
2. $r_s > 0$, $r_l = 0$.—Extended source, unocculted (Witt & Mao 1994).
3. $r_s > 0$, $1 > r_l > 0$.—Extended source, inner image may be partly occulted, outer image unocculted.

TABLE 1
MAGNIFICATION OF INNER IMAGE

Case	r_l	r_s	ζ_0	$\mu_-(\zeta_0)$
I............	0	0	$(0, \infty)$	μ_-^p
	$(0, 1)$	0	$(0, \beta_l)$	
II...........	$(0, 1)$	$(0, \infty)$	$[\beta_l + r_s, \infty)$	0
	$[1, \infty)$	$[0, \infty)$	$[0, \infty)$	
III	0	$(0, \infty)$	$[0, r_s)$	μ_-^e
	0	$(0, \infty)$	(r_s, ∞)	
	$(0, 1)$	$(0, \beta_l)$	$(r_s, \beta_l - r_s]$	
	$(0, 1)$	$(0, \beta_l)$	$[0, r_s)$	
IV	0	$(0, \infty)$	r_s	$\mu_-^{e,*}$
	$(0, 1)$	$(0, \beta_l/2]$	r_s	
V...........	$(0, 1)$	$[\beta_l, \infty)$	$(r_s, \beta_l + r_s)$	μ_-^o
	$(0, 1)$	$[\beta_l, \infty)$	$(r_s - \beta_l, r_s)$	
	$(0, 1)$	$(0, \beta_l)$	$(\beta_l - r_s, \beta_l + r_s)$	
VI	$(0, 1)$	$(\beta_l/2, \infty)$	r_s	$\mu_-^{o,*}$
VII	$(0, 1)$	$[\beta_l, \infty)$	$[0, r_s - \beta_l]$	$(1 - r_l^2)/r_s^2$

4. $r_s > 0$, $r_l > 1$.—Extended source, inner image fully occulted, outer image may be partly occulted.

The expressions for $\mu_\pm$ in each of these cases are summarized in Tables 1 and 2, where p, e, and o superscripts refer to the point-source magnification (Paczyński 1986), extended-source magnification (Witt & Mao 1994), and occulted-extended source magnification (below), respectively, and $\beta_l = |r_l^{-1} - r_l|$. Each of the magnification expressions in Tables 1 and 2 is given in equations (5) and (17)–(25), with the range of the variables for which the functions apply given in the columns.

As an example of how the computation proceeds, we consider the case in which $r_l > 1$ and the source overlaps the shadow of the lens (for example, the source in Fig. 1d at $x = 0.6$). In this case, the inner image is completely occulted while the outer image is partially occulted, so we must integrate equation (13) for ϕ between $\pm\chi = \pm\cos^{-1}\left[\left(\beta_l^2 - r_s^2 - \zeta_0^2\right)/(2 r_s \zeta_0)\right]$. This gives an area that is between the outer edge of the source image and the origin, so we need to subtract off the area within the shadow that is $r_l^2 \phi_2 = r_l^2 \cos^{-1}\left[\left(r_s^2 - \beta_l^2 - \zeta_0^2\right)/(2\beta_l \zeta_0)\right]$. Thus,

$$\mu_+^o = \frac{1}{\pi r_s^2} \int_{-\chi}^{\chi} d\phi |z_\pm|^2 \frac{\partial \Psi}{\partial \phi} - \frac{\phi_2 r_l^2}{\pi r_s^2} . \tag{15}$$

Making the substitution $u = \beta^2 = \zeta_0^2 + r_s^2 + 2\zeta_0 r_s \cos\phi$, this

TABLE 2
MAGNIFICATION OF OUTER IMAGE

Case	r_l	r_s	ζ_0	$\mu_+(\zeta_0)$
I.........	$[0, 1)$	0	$(0, \infty)$	μ_+^p
	$[1, \infty)$	0	(β_l, ∞)	
II........	$[1, \infty)$	$(0, \beta_l]$	$[0, \beta_l - r_s]$	0
III	$[0, 1)$	$(0, \infty)$	$[0, r_s)$	μ_+^e
	$[0, 1)$	$(0, \infty)$	(r_s, ∞)	
	$[1, \infty)$	$(0, \infty)$	$[\beta_l + r_s, \infty)$	
IV	$[0, 1)$	$(0, \infty)$	r_s	$\mu_+^{e,*}$
V........	$[1, \infty)$	$(0, \infty)$	$(\lvert r_s - \beta_l \rvert, \beta_l + r_s)$	μ_+^o
VI	$[1, \infty)$	(β_l, ∞)	$[0, r_s - \beta_l]$	$\mu_+^e + (1 - r_l^2)/r_s^2$

equation is

$$\mu_+^o = \frac{1}{4\pi r_s^2}\int_{\beta_l^2}^{u_2} du\, \frac{(u-u_3)\left[1+2u^{-1}+\sqrt{(4+u)/u}\right]}{\left[(u_2-u)(u-u_1)\right]^{1/2}} - \frac{\phi_2 r_l^2}{\pi r_s^2}\ , \tag{16}$$

where u_1, u_2, and u_3 are defined below. The integral can be reduced to elliptic integrals as given below.

For an extended source ($r_s > 0$), the magnification of the inner image when $1 > r_l > 0$ is given by

$$\mu_-^o = \frac{\Theta(r_s-\zeta_0)}{r_s^2} - \frac{1}{4\pi r_s^2}\left[2(1+r_s^2)\phi_1 - 4\,\mathrm{sgn}\,(u_3)\phi_0 + 4r_l^2\phi_2 + \sqrt{(u_2-u_0)(u_0-u_1)}\left(\sqrt{1+\frac{4}{u_0}}-1\right) - G(\phi_0)\right]\ , \tag{17}$$

where

$$G(\phi) = \frac{1}{\sqrt{u_2(4+u_1)}}\left[u_2(4+u_1)E(\phi,\ k_1) - (u_1u_2+8u_3)F(\phi,\ k_1) + 4u_1(1+r_s^2)\Pi(\phi,\ n,\ k_1)\right]\ , \tag{18}$$

F, E, and Π are elliptic integrals of the first, second, and third kinds (Gradshteyn & Ryzhik 1994), sgn (x) chooses the sign of x, and the other variables are

$$\begin{aligned} u_0 &= \beta_l^2, \quad u_1 = (\zeta_0 - r_s)^2\ ,\\ u_2 &= (\zeta_0+r_s)^2, \quad u_3 = \zeta_0^2 - r_s^2\ ,\\ \phi_0 &= \cos^{-1}\sqrt{\frac{u_1(u_2-u_0)}{u_0(u_2-u_1)}}\ ,\\ \phi_1 &= \cos^{-1}\left(\frac{u_1+u_2-2u_0}{u_2-u_1}\right)\ ,\\ \phi_2 &= \cos^{-1}\left(\frac{u_3+u_0}{2\zeta_0 u_0^{1/2}}\right)\ ,\\ n &= 1-\frac{u_1}{u_2}, \quad k_1^2 = \frac{4(u_2-u_1)}{u_2(4+u_1)}\ . \end{aligned} \tag{19}$$

In the special case that $\zeta_0 = r_s$, the magnification of the inner image becomes

$$\mu_-^{o,*} = \mu_-^{e,*} + \frac{1}{\pi r_s^2}\left[\left(1+r_s^2-r_l^2\right)\cos^{-1}\frac{\beta_l}{2r_s} + \frac{v_2}{4}(\beta_l - v_1) - (1+r_s^2)\tan^{-1}\frac{v_2}{v_1}\right]\ , \tag{20}$$

where

$$v_1 = \sqrt{4+\beta_l^2}, \quad v_2 = \sqrt{4r_s^2 - \beta_l^2}\ , \tag{21}$$

and

$$\mu_\pm^{e,*} = \frac{1}{\pi r_s^2}\left[r_s + (1+r_s)^2\tan^{-1} r_s\right] \pm \frac{1}{2}\ , \tag{22}$$

which is the magnification of the unocculted images when $\zeta_0 = r_s$.

When $r_l > 1$, then the outer image can be occulted. The magnification in this case is given by

$$\mu_+^o = \frac{1}{4\pi r_s^2}\left[2\left(1+r_s^2\right)\psi_2 - 4\,\mathrm{sgn}\,(u_3)\psi_1 - 4r_l^2\phi_2 + \sqrt{(u_2-u_0)(u_0-u_1)}\left(\sqrt{\frac{u_0}{4+u_0}}+1\right) + G(\psi_0)\right]\ , \tag{23}$$

where

$$\begin{aligned} \psi_0 &= \cos^{-1}\sqrt{\frac{(u_0-u_1)(4+u_2)}{(4+u_0)(u_2-u_1)}}, \quad \psi_1 = \frac{\pi}{2} - \phi_0\ ,\\ \psi_2 &= \pi - \phi_1 + 2\cos^{-1}\sqrt{\frac{u_0(4+u_0)}{u_0(4+u_1+u_2)-u_1u_2}}\ , \end{aligned} \tag{24}$$

and the other variables are as in equation (19).

When the inner or outer images are unocculted, then the magnification is

$$\mu_-^e = \frac{G(\pi/2)}{4\pi r_s^2} - \frac{1}{2}, \quad \mu_+^e = \frac{G(\pi/2)}{4\pi r_s^2} + \frac{1}{2}\ , \tag{25}$$

which agrees with the expression of Witt & Mao (1994). In principle, one could also compute the image centroid for the source including occultation (as done by Witt 1995).

We now provide several graphical examples of these equations. Figure 2 shows the magnification for a source with $r_l = 0.9$ and $r_s = 0.25$, compared to cases in which either $r_l = 0$ or $r_s = 0$. In all three cases, the outer image is unobscured, but the inner image appears when the source approaches the lens. In the point-source case, the appearance is abrupt and creates a strong brightening, while for the extended source, the appearance is more gradual.

Figure 3 shows the magnification for a source with $r_l = 1.1$ and $r_s = 0.25$, compared to cases in which either $r_l = 0$ or $r_s = 0$. The finite size of the lens and the source cre-

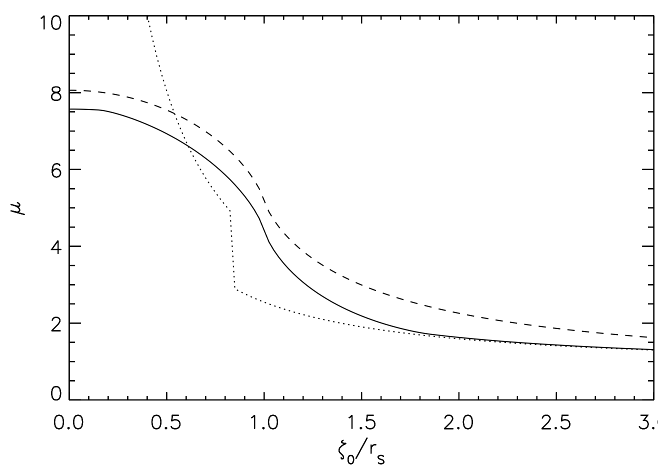

FIG. 2.—Magnification for $r_s = 0.25$, $r_l = 0.9$ (*solid line*), $r_s = 0$, $r_l = 0.9$ (*dotted line*; in this case, the horizontal axis is scaled by $r_s = 0.25$ for comparison), and $r_s = 0.25$, $r_l = 0$ (*dashed line*).

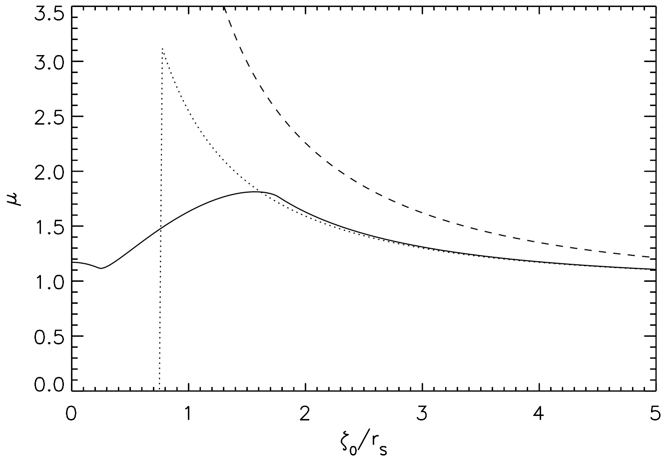

FIG. 3.—Magnification for $r_s = 0.25$, $r_l = 0.9$ (*solid line*), $r_s = 0$, $r_l = 0.9$ (*dotted line*; in this case, the horizontal axis is scaled by $r_s = 0.25$ for comparison), and $r_s = 0.25$, $r_l = 0$ (*dashed line*).

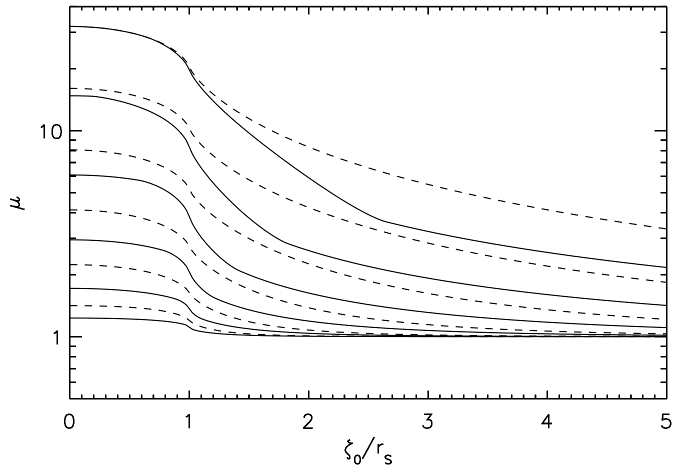

FIG. 5.—Magnification for $r_s = 1/16$, $1/8$, $1/4$, $1/2$, 1, and 2 (*top to bottom*). Solid lines show $r_l = 0.95$, while dashed lines show $r_l = 0$.

ates both magnification and occultation, but the magnification wins out ($\mu > 1$) in this case. In all three cases, the inner image is obscured, while the outer image can be obscured when the source approaches the lens. In the point-source case, the occultation is abrupt and results in the disappearance of the background source.

For the case of $r_s = 1$, we show several different values of r_l in Figure 4. In all cases with finite r_l, the magnification shows a much flatter profile near the origin than for the $r_l = 0$ case. In the limit $r_l \ll 1$, the light curve approaches that of extended-source microlensing, while for $r_l \gg 1$, it approaches the limit of occultation.

Figure 5 shows magnification for different source sizes, but a fixed lens size $r_l = 0.95$. The smallest sources show broad sloping wings, indicative of the appearance of the second image; in the smallest case, the source becomes completely revealed near the origin. For the largest cases, the magnification shows a sharper slope near $\zeta_0 = r_s$ than in the $r_l = 0$ case.

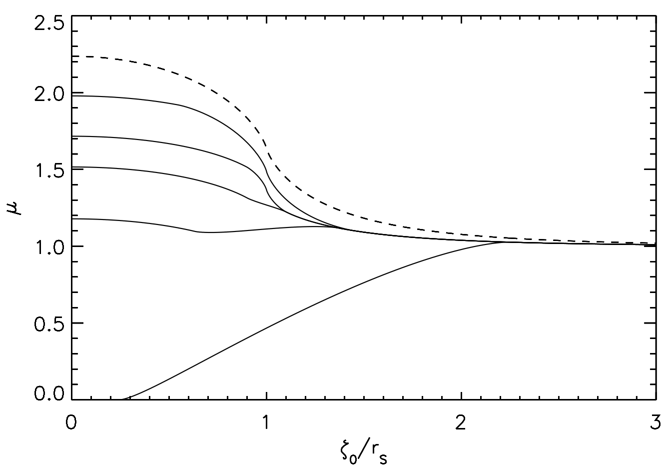

FIG. 4.—Magnification for $r_s = 1$ and $r_l = 0.8$, 0.95, 1.05, 1.2, and 1.8 (*solid lines, top to bottom*). The dashed line shows $r_l = 0$.

A uniform source causes rather sharp features in the light curve during the ingress and egress of the occultation and leads to flatter light curves during transit. However, a limb-darkened source has a smoother ingress/egress and has curvature during transit. Thus, in § 4 we consider microlensing and occultation of a limb-darkened source.

4. LIMB DARKENING

Limb darkening causes a star to be more centrally peaked in brightness compared to a uniform source. This leads to larger magnification during microlensing or larger dimming during transit/occultation. Thus, including limb darkening is important for computing accurate microlensing/occultation light curves. Describing limb darkening with a quadratic law,

$$\frac{I(r)}{I(0)} = 1 - \gamma_1(1-\sigma) - \gamma_2(1-\sigma)^2 \ ,$$
$$\sigma = \sqrt{1 - \left(\frac{r}{r_s}\right)^2} \ , \tag{26}$$

where $\gamma_1 + \gamma_2 < 1$, leads to a magnification of

$$\mu(r_l,\ r_s,\ \zeta_0,\ \gamma_1,\ \gamma_2) = \frac{\int_0^{r_s} dr\, I(r)(d\mu r^2/dr)}{\int_0^{r_s} dr\, 2rI(r)} \ , \tag{27}$$

where $\mu(r)$ can be computed from the expressions in § 3 (replacing r_s with r). We could use a more accurate limb-darkening formula but rely on a quadratic law for simplicity. Given the complicated dependence of the magnification on the radius, this integral is best done numerically using a finite-difference approximation for the derivative of the uniform magnification. An example is shown in Figure 6; in this case, the dip during occultation is deeper due to limb darkening, since the source is brighter at the center, and thus more flux is lost, and the magnification decreases toward the origin rather than increasing as in the uniform-source case. Both the uniform and the limb-darkened cases are shallower when compared to the pure-occultation case due

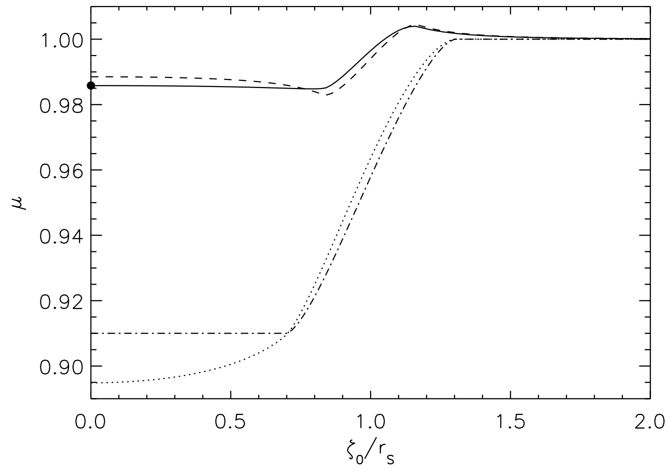

FIG. 6.—Magnification for $r_s = 5$ and $r_l = 1.5$. The solid line shows limb darkening with $\gamma_1 = \gamma_2 = 0.3$ (eq. [27]), while the dashed line shows a uniform source (eq. [14], Tables 1 and 2). The dot-dashed line shows a uniform source and a lens of the same size ratio but neglecting lensing, while the dotted line shows a limb-darkened source neglecting lensing. The filled circle on the y-axis shows the result of eq. (28).

to magnification of the background source. A second example is shown in Figure 7. In this case, the limb darkening causes a weaker magnification as the outer limb is magnified, while the peak is increased because of the more concentrated brightness. In the special case in which $\zeta_0 = 0$, the integral is tractable analytically as follows and is shown as the filled circles in Figures 6 and 7.

For $r_l > 0$ and $r_s > \beta_l$, the magnification for a limb-darkened source at $\zeta_0 = 0$ becomes

$$\mu = \frac{\sqrt{4+r_s^2}}{6\Omega r_s^3}\left\{\alpha_1\left[(2+r_s^2)E(\phi_3,\ k_2) - 2F(\phi_3,\ k_2)\right] + \alpha_2 r_s\right\} + \frac{1}{6\Omega r_s^3}\left[s\beta_l(4+\beta_l^2)^{1/2} + \alpha_3\right]\left(\alpha_1\sqrt{\alpha_3} + \alpha_2 - \frac{3\gamma_2}{2r_s}\alpha_3\right) + \frac{2\gamma_2}{r_s^4\Omega}\left[\frac{\alpha_3}{8}(2+r_s^2) + \sinh^{-1}\left(\frac{r_s}{2}\right) + \sinh^{-1}\left(\frac{s\beta_l}{2}\right)\right]\ , \tag{28}$$

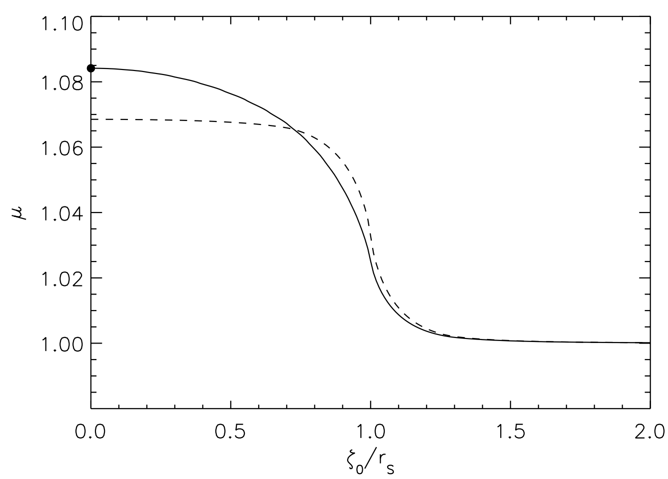

FIG. 7.—Magnification for $r_s = 5$ and $r_l = 0.5$. The solid line shows limb darkening with $\gamma_1 = \gamma_2 = 0.3$, while the dashed line shows a uniform source. The filled circle on the y-axis shows the result of eq. (28).

where

$$\begin{aligned}
\alpha_1 &= 2(\gamma_1 + 2\gamma_2)\ , \\
\alpha_2 &= 3(1-\gamma_1-\gamma_2)r_s - \frac{3\gamma_2}{2r_s}(2+r_s^2)\ , \\
\alpha_3 &= r_s^2 - \beta_l^2, \quad \Omega = 1 - \frac{\gamma_1}{3} - \frac{\gamma_2}{6}\ , \\
\phi_3 &= \cos^{-1}\left(-s\frac{\beta_l}{r_s}\right), \quad s = \mathrm{sgn}\,(1-r_l)\ , \\
k_2^2 &= \frac{r_s^2}{4+r_s^2}\ .
\end{aligned} \tag{29}$$

When $\phi_3 > \pi/2$, then $E(\phi_3,\ k_2) = 2E(k_2) - E(\pi - \phi_3,\ k_2)$ and $F(\phi_3,\ k_2) = 2K(k_2) - F(\pi - \phi_3,\ k_2)$. For $r_l < 1$ and $r_s < \beta_l$, the inner image is unocculted (the latter is always true for $r_l = 0$), and β_l should be replaced by r_s in equations (28) and (29) to give

$$\mu = \frac{1}{\Omega r_s^2}\left\{\frac{\alpha_1}{3k_2}\left[(2+r_s^2)E(k_2) - 2K(k_2)\right] + \frac{\alpha_2 r_s}{3k_2} + \frac{4\gamma_2}{r_s^2}\sinh^{-1}\left(\frac{r_s}{2}\right)\right\}\ . \tag{30}$$

For $\gamma_2 = 0$, this expression agrees with equation (A6) in Witt (1995).

In the occultation limit when the Einstein radius is small, $R_{\rm E} \ll R_l$, R_s, then the light curve can be described by occultation only. We can include limb darkening exactly in this case (K. Mandel & E. Agol 2002, in preparation). An example is shown in Figure 6 of the difference between occulting and micro-occulting light curves.

5. DISCUSSION

The equations for micro-occultation are most relevant for equality of the Einstein radius and lens radius, which occurs if $D \equiv D_l(D_s - D_l)/D_s = R_l^2/(4R_g)$. We compute D for several interesting objects in Table 3 (not to be confused with their actual distances), including a white dwarf (Sirius B), brown dwarf (Gliese 229b), red giant (Capella), blue supergiant (Rigel), yellow supergiant (Deneb), and red supergiant (Betelgeuse). Application of the micro-occultation equations to white dwarfs, brown dwarfs, nearby supergiants, and giants in globular clusters are discussed next.

White dwarfs in eclipsing binaries are the most likely location to see micro-occultation (Maeder 1973; Marsh 2001). Known white dwarf binaries that transit their companions have small semimajor axes (likely a selection effect),

TABLE 3

DISTANCE FOR WHICH $R_{\rm E} = R_l$

Object	$M/M_\odot$	$R_L/R_\odot$	D
Sirius B	1	0.009	0.04 AU
Gliese 229B	0.05	0.1	100 AU
Sun	1	1	550 AU
Jupiter..............	10^{-3}	0.1	0.03 pc
Earth	3×10^{-6}	0.01	0.07 pc
Rigel	20	36	0.2 pc
Deneb	14	60	0.7 pc
Pluto	6×10^{-9}	0.0017	1 pc
Betelgeuse	20	10^3	133 pc

and thus small Einstein radii, changing the depth of transit by only a few percent (Marsh 2001). Due to common-envelope evolution, white dwarf binaries have typical semimajor axes $a \sim 0.1$ AU and masses of 0.5 $M_\odot$, so $R_{\rm E} \sim 7 \times 10^8\ {\rm cm}(M/0.5\ M_\odot)^{1/2}(a/0.1\ {\rm AU})^{1/2}$. This is comparable to the size of white dwarfs, $\sim 10^9$ cm, so both occultation and microlensing are important. A. Farmer, E. Agol, & S. Wyithe (2002, in preparation) apply the formulae derived here to estimate how many white dwarfs can be found in transit searches for extrasolar planets. For example, the Kepler survey (Koch et al. 1998) may find ∼10–100 white dwarfs, comparable to the expected number of terrestrial planets. White dwarf transit events require the inclusion of both lensing and occultation in modeling the light curves.

Although smaller in mass, brown dwarfs in eclipsing binaries may have some observable microlensing effects during eclipse. As gas planets and brown dwarfs have very similar sizes, their transits of companion stars may look quite similar. However, in the limit of a large source, the depth of the transit scales as $1 + 2(R_{\rm E}/R_s)^2 - (R_l/R_s)^2$ (for a uniform source), so brown dwarfs have a transit of smaller depth, since $R_{\rm E}$ is larger. This affects the measurement of limb darkening, which also changes the depth of the transit (eq. [28]). In the case of a 0.05 $M_\odot$ brown dwarf with radius 0.1 $R_\odot$ in orbit at 1 AU about a G-type star, $r_l = 10$ and $r_s = 10^2$. Thus, the transit depth differs by 2×10^{-4} from a 10^{-3} $M_\odot$ planet of the same radius. Such photometric precision can be obtained with the *Hubble Space Telescope*; (Brown et al. 2001) and other planned satellites and is indicated by a slight brightening outside of the transit (Fig. 6). The difference can be much larger, ∼1%, if the primary is also a brown dwarf.

Lensing events caused by nearby stars may also show the signs of both microlensing and occultation. The most extreme case is the star Betelgeuse, which has a distance of ∼125 pc and a mass of ∼20 $M_\odot$, giving an Einstein radius of 7×10^{13} cm for sources at a much larger distance. This is only slightly larger than the size of Betelgeuse, $\sim 4 \times 10^{13}$ cm, so that distant stars passing behind Betelgeuse would create two visible images as they approach; a full occultation would never occur (unless the mass of Betelgeuse were much smaller). Distant galaxies would create an Einstein ring surrounding the star with the center occulted. The challenge involved in carrying out such an observation is in resolving a faint background source from the bright foreground star and waiting long enough for Betelgeuse to pass in front of a star or galaxy. In every microlensing event, an occultation should occur when $\beta = \beta_l$. Since this usually leads to a demagnified image, extremely accurate photometry is necessary to see an occultation event.

A final application of the micro-occultation equations is to giant stars acting as lenses in globular clusters. There are about 3×10^5 evolved giant stars in Milky Way globular clusters. For a giant star in a clump with a mass of 1 $M_\odot$, the Einstein radius for a separation of 1 pc is ∼20 $R_\odot$, comparable to the size of the star, ∼20 $R_\odot$. If the relative velocity is ~ 10 km s^{-1}, then red giants in globular clusters cover about 3×10^{31} cm^2 yr^{-1}, which is about 10^{-8} of the total area in globular clusters. Thus, about 10^8 stars in globular clusters must be monitored to find a single red giant transit event per year, and a typical event will last about one month. A light curve of a lensing event by a red giant in a globular cluster would allow one to measure r_l and r_s, as well as γ_1 and γ_2, for the source star. Since the Einstein radius in this case is $R_{\rm E} = (4GMc^{-2}D)^{1/2}$, where D is the separation of the lenses in the cluster, one can estimate the surface gravity of the lens giant, $g = GM/R_l^2 \sim c^2/(4D)$ (Bromley 1996), given that D will be of the order of the scale length of the globular cluster.

6. CONCLUSIONS

We have computed exact formulae for the lensing of a uniform extended source by an opaque, spherical lens (with escape velocity much smaller than c). The formulae only differ significantly from the usual occultation or microlensing formulae in the limit that $R_l \sim R_{\rm E}$, which may be relevant for lensing by white dwarfs in binaries or lensing by giant stars. Small deviations due to lensing in eclipsing brown dwarf binaries may be detectable with very precise photometry, which may be another application of the expressions derived here. A code written in IDL that carries out the calculations presented here can be downloaded from on-line.[3]

We thank Sara Seager for useful discussions and comments on a draft. Support for E. A. was provided by the National Aeronautics and Space Administration through *Chandra* postdoctoral fellowship award PF0-10013 issued by the Chandra X-Ray Observatory Center, which is operated by the Smithsonian Astrophysical Observatory for and on behalf of the National Aeronautics Space Administration under contract NAS 8-39073.

[3] See http://www.pha.jhu.edu/∼agol.

REFERENCES

Bozza, V., Jetzer, Ph., Mancini, L., & Scarpetta, G. 2002, A&A, 382, 6
Bromley, B. 1996, ApJ, 467, 537
Brown, T. M., Charbonneau, D., Gilliland, R. L., Noyes, R. W., & Burrows, A. 2001, ApJ, 552, 699
Dominik, M. 1998, A&A, 333, L79
Gould, A., & Gaucherel, C. 1997, ApJ, 477, 580
Gradshteyn, I. S., & Ryzhik, I. M. 1994, Tables of Integrals, Series, and Products (New York: Academic)
Koch, D., Borucki, W., Webster, L., Dunham, E., Jenkins, J., Marriott, J., & Reitsema, H. 1998, Proc. SPIE, 3356, 599
Maeder, A. 1973, A&A, 26, 215
Marsh, T. R. 2001, MNRAS, 324, 547
Paczyński, B. 1986, ApJ, 304, 1
Schneider, P., Ehlers, J., & Falco, E. E. 1992, Gravitational Lenses (New York: Springer)
Walker, M. 1995, ApJ, 453, 37
Witt, H. J. 1995, ApJ, 449, 42
Witt, H. J., & Mao, S. 1994, ApJ, 430, 505